Impact of skin pigmentation on photoacoustic imaging using linear array transducer: a pilot in vivo study

Guilherme S. Pilotto Fernandes*, Joao H. Uliana*, Luciano Bachmann*, Antonio A. O Carneiro*, Muyinatu A. Lediju Bell†‡§ and Theo Z. Pavan*

*Department of Physics, Faculty of Philosophy, Sciences and Letters of Ribeirao Preto, University of Sao Paulo, Brazil

†Department of Electrical and Computer Engineering, Johns Hopkins University, Baltimore, MD, United States

‡Department of Biomedical Engineering, Johns Hopkins University, Baltimore, MD, United States

§Department of Computer Science, Johns Hopkins University, Baltimore, MD, United States

2022 IEEE International Ultrasonics Symposium (IUS) | 978-1-6654-6657-8/22/$31.00 ©2022 IEEE | DOI: 10.1109/IUS54386.2022.9958826

***Abstract*—Clinical photoacoustic (PA) imaging systems commonly integrate illumination and detection into the same probe. In this case, PA waves originating from light absorption by melanin in the skin propagate into the tissue and are backscattered to the transducer, which introduces acoustic clutter artifacts. In addition, skin absorption also decreases light fluence within the imaging plane. Therefore, it is important to understand how the amount of melanin in the epidermis impacts PA imaging quality. Toward this goal, PA images of 10 volunteers with different skin constitutive pigmentation were acquired with laser wavelengths of 750 nm, 810 nm, and 870 nm. The radial artery was adopted as the reference to calculate signal-to-noise ratios (SNRs) in order to quantify the presence of clutter artifacts in conventional amplitude-based PA images, as well as the capability of reducing clutter by applying short-lag spatial coherence (SLSC) beamforming. With conventional amplitude-based beamforming, the mean SNR across the 10 volunteers decreased from 38.9 dB to 33.7 dB with the decreasing epidermal melanin content. However, the mean SNR improved by 4.2 dB with SLSC PA images compared to conventional PA images. Overall, SLSC beamforming successfully reduced the appearance of clutter artifacts in PA images, resulting in better visualization of the radial artery and improved image quality. These results are promising to implement SLSC to both reduce acoustic clutter and improve target visualization in photoacoustic images acquired with light transmission through darker skin tones.**

***Index Terms*—photoacoustic imaging, clutter artifact, melanin, short-lag spatial coherence, skin pigmentation, image quality, ultrasound**

I. Introduction

Photoacoustic (PA) imaging using linear array transducers has traditionally adopted the reflection mode acquisition, where optical fibers are attached to the ultrasound transducer to illuminate the tissue [1], [2]. In this case, the illumination beam first strikes the skin, which can be characterized by high optical absorption coefficients in the visible and near-infrared range, due to the melanin content in the epidermis layer [3], [4]. This light absorption can considerably affect the illumination efficiency, particularly for deep-located structures in the imaging plane. In addition, the PA waves generated due to light absorption at the skin surface can also be a source of acoustic clutter artifacts [5]–[7].

In ultrasound imaging, the clutter artifact originates from the interaction between the acoustic wave and the surrounding media (reverberation and scattering) [8]. This artifact can have, for example, a negative impact on several clinical ultrasound imaging applications such as vascular [9], cardiac [10], abdominal [11] and breast [12]. In the case of PA imaging, PA waves generated by strong optical absorbers interact with the surrounding media. The scattered waves that travel back to the ultrasound transducer can be interpreted as PA signal, but this "signal" is actually an artifact known as acoustic clutter. This artifact increases the background signal level causing misinterpretation of the real PA signals from absorbers within the tissues, which deteriorates the signal-to-noise ratio (SNR), contrast, and imaging depth [13]. Mantri *et al* [6] verified that skin pigmentation can affect PA-based oxygen saturation estimation and Li *et al* [7] showed that the total blood volume calculated for individuals with high melanin content needs to be compensated. Therefore, it is important to understand how the epidermal melanin content impacts PA images acquired with light illuminating skin tissue.

The skin pigmentation of an individual is well correlated with the epidermal melanin content [14]. A quantitative measurement of skin pigmentation is the individual typology angle (ITA°) [15]. According to ITA° values, the skin color can be classified as very light, light, intermediate, tan, brown or dark [15]. In this case, very light and dark skin color presents lower and higher melanin content, respectively. Thus, PA images from darker skin individuals are expected to be more affected by clutter artifacts, in addition to suffering from lower light fluence within the imaging plane. Both of these effects compound to compromise the resulting PA image quality.

Previous studies have shown that the short-lag spatial coherence (SLSC) beamforming is capable of reducing clutter in PA images and can improve image quality in low light fluence and noisy environments [16]. SLSC computes the spatial coherence between received signals at different transducer elements separation M and sums across the M values to generate the image [17]. Because clutter sources have low spatial coherence, acoustic clutter artifacts that appear in

TABLE I
VOLUNTEERS INFORMATION

Volunteer Number	Age [years]	Weight [kg]	Height [m]	ITA°	Skin Color
1	26	85	1.80	46.44	Light
2	21	60	1.85	42.68	Light
3	30	77	1.76	32.41	Intermediate
4	30	77	1.74	29.18	Intermediate
5	29	84	1.76	19.73	Tan
6	30	69	1.78	12.39	Tan
7	23	86	1.85	-6.43	Brown
8	41	72	1.76	-6.53	Brown
9	40	100	1.70	-33.57	Dark
10	38	77	1.70	-53.74	Dark

TABLE II
SKIN COLOR CLASSIFICATION

Grading	ITA	Skin Color Category
I	$> 55°$	Very Light
II	$> 41° and \leq 55°$	Light
III	$> 28° and \leq 41°$	Intermediate
IV	$> 10° and \leq 28°$	Tan
V	$\leq -30° and \leq 10°$	Brown
VI	$< -30°$	Dark

traditional PA images tend be mitigated in SLSC images due to the lower SLSC pixel values [18]–[21]. This approach can also be implemented in real time [22].

Therefore, in this study, PA data of the distal forearm from individuals with different skin constitutive pigmentation levels were acquired with optical wavelengths of 750 nm, 810 nm, and 870 nm in order to understand the impact of the epidermal melanin content on conventional amplitude-base PA images as well as the capability of reducing various clutter artifacts produced by different skin pigmentation levels after applying SLSC beamforming.

II. MATERIALS AND METHODS

A. Volunteers

A total of 10 volunteers were included in this study. The skin color of the volunteers was classified as follows: light (n = 2), intermediate (n = 2), tan (n = 2), brown (n = 2) and dark (n = 2) . Additional information about each volunteer is summarized in Table I. These experiments were conducted with approval from the USP Research Ethical Committee (CAAE: 08860819.4.0000.5407).

B. Skin Color Classification

Prior to the acquisition of PA images, a depilatory cream (Needs Depil Aloe Vera) was applied on the imaging region in order to minimize the presence of hair at the skin's surface. Then, the $L^*a^*b^*$ values were measured using a colorimeter (Delta Vista 450G) and the ITA° was calculated using (1) to classify the volunteer skin color as described in Table II.

$$\text{ITA}^\circ = \tan^{-1}\left(\frac{L^* - 50}{b^*}\right) \cdot \left(\frac{180^\circ}{\pi}\right) \quad (1)$$

C. Imaging System

The PA system consisted of a Nd:YAG laser (Brilliant B, Quantel Laser) coupled to an optical parametric oscillator (OPO) (MagicPRISM, Opotek) and a trifurcated optical fiber bundle (77536, Newport) attached to a linear array transducer (L14-5/38, Ultrasonix). The transducer was connected to a commercial ultrasound machine (SonixOP, Ultrasonix) with a parallel acquisition module (SonixDAQ, Ultrasonix). Two beamformers were applied to reconstruct the images: i) conventional amplitude-based, obtained using a single step reconstruction technique based on the fast Fourier transform (FFT) [23] and ii) coherence-based technique, obtained using the SLSC beamforming [17]. The radial artery was adopted as the reference to calculate SNR for both FFT PA and SLSC images according to the following equation:

$$SNR = 20 \cdot \log_{10}\left(\frac{s_i}{\sigma_0}\right)[dB], \quad (2)$$

where s_i is the mean signal from the radial artery and σ_0 is the background standard deviation.

III. RESULTS AND DISCUSSION

Before the acquisition of PA data, B-mode images were acquired to ensure the radial artery was located within the imaging plane. Figure 1 shows an example of ultrasound B-mode image (gray scale) overlaid by the color-encoded SLSC PA image for Volunteer 1 (light skin color), obtained with a laser wavelength of 870 nm.

Figure 2 shows the FFT and SLSC PA images for Volunteers 1 (light skin color) and 10 (dark skin color), acquired with 750 nm and 870 nm optical wavelengths. The radial artery location is indicated by the green arrows. The PA signal amplitude associated with the skin decreased as wavelength increased for both volunteers, likely because the optical absorption coefficient of melanin is lower for higher wavelengths in the near infrared region [3]. Minimal acoustic clutter is present in the FFT PA images of Volunteer 1 (light skin color) acquired with optical wavelengths of 750 nm and 870 nm. Therefore, the visualization of the radial artery was not compromised. However, the clutter artifact was considerably increased for the volunteer with darker skin color, particularly when acquired with the 750 nm optical wavelength. In this case, it is not possible to visualize the radial artery due to the strong clutter artifact present in the conventional amplitude-based PA image. For this volunteer, the clutter artifact level

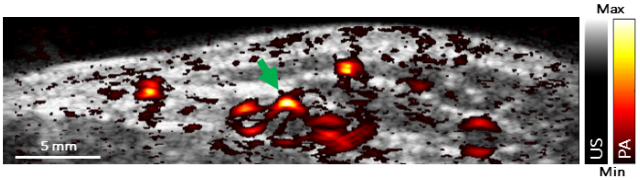

Fig. 1. B-mode image (gray scale) overlaid by the color-encoded SLSC PA image from volunteer 1. The green arrow indicates the radial artery position on the image.

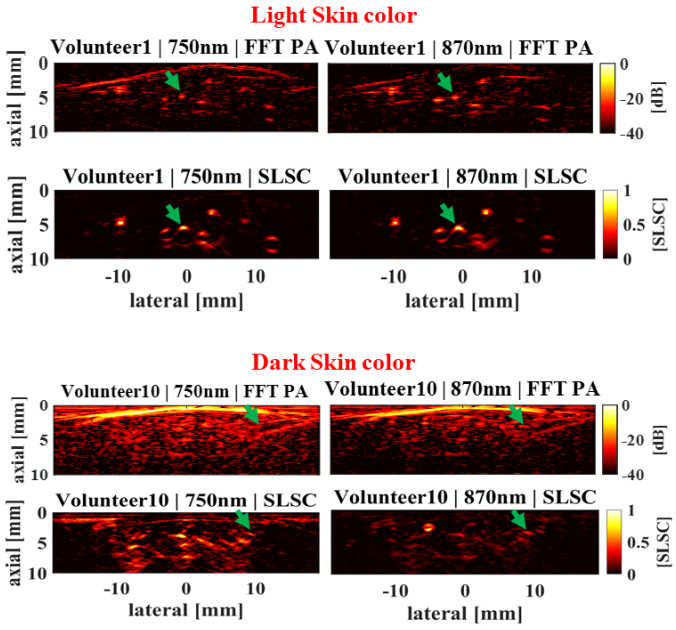

Fig. 2. FFT and SLSC PA images for volunteers 1 and 10 (light and dark skin color, respectively). Green arrows indicate radial artery position on images.

was lower for the image at 870 nm, but the reduced light fluence still compromised the radial artery visualization in the amplitude-based PA image. The SLSC images present an important clutter artifact reduction, resulting in considerably improved radial artery visualization. PA images of good visual quality, for both light and dark skin color volunteers, were achieved with 870 nm wavelength when SLSC beamforming was employed.

Figure 3 illustrates the SNR improvement achieved with SLSC compared to FFT PA images, by displaying the mean SNR values calculated for the ten volunteers, grouped by skin color category and wavelengths. As expected, images obtained with 750 nm wavelength produced lower SNR values, given that for this wavelength clutter artifacts are more prominent and the light fluence within the imaging plane is lower due to the high optical absorption coefficient of the epidermis. In addition, the signal from the radial artery is expected to be lower at 750 nm compared to 870 nm, due to the absorption coefficient spectrum for oxygenated blood [3]. SNR consistently decreased as skin color progressed to darker colors for both FFT and SLSC PA images and for the three wavelengths investigated. This trend is supported by darker skin containing higher melanin content, which increases optical absorption by the skin. For the three wavelengths and for each skin pigmentation investigated, SNR was improved in the SLSC images when compared to FFT PA images.

Figure 4 shows the mean SNR calculated from the SLSC images for the ten volunteers, stratified by skin color category and optical wavelengths. This result highlights the SNR increase with increased optical wavelengths and the SNR decrease with increased melanin content.

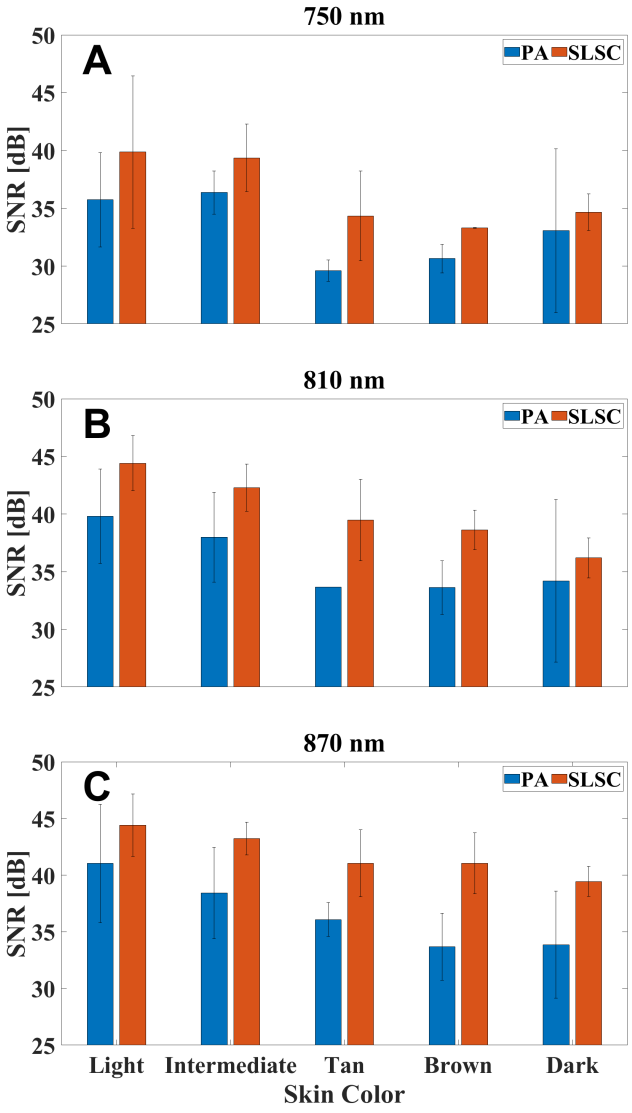

Fig. 3. Mean SNR values calculated for the 10 volunteers when PA images were created with amplitude-based FFT and SLSC, acquired with optical wavelengths of A) 750 nm, B) 810 nm, and C) 870 nm.

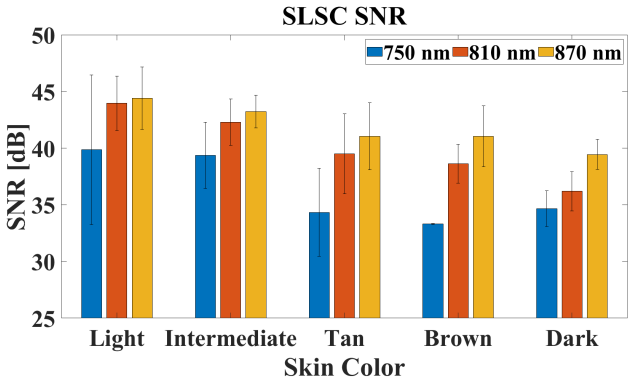

Fig. 4. Mean ± one standard deviation of SNR measured in SLSC images of the 10 volunteers, acquired with optical wavelengths of 750 nm, 810 nm, and 870 nm.

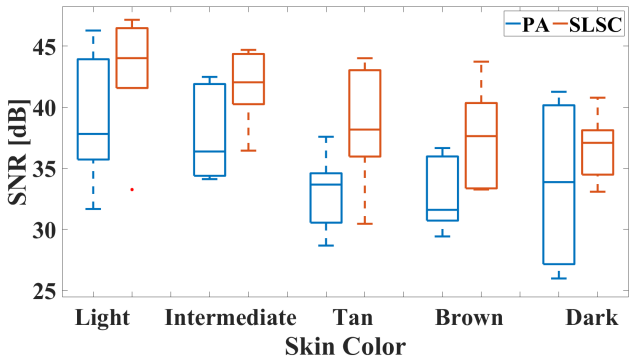

Fig. 5. Boxplots showing the SNR values obtained from the three wavelengths investigated for the ten volunteers, stratified by skin category and FFT or SLSC image formation methods.

To understand the impact of epidermal melanin content on PA image quality, Figure 5 shows the distribution of SNR values calculated from the ten volunteers distributed among the various skin color categories for the three wavelengths combined, offering a direct comparison of FFT and SLSC PA results. Although both image formation techniques resulted in lower SNR with greater melanin content, the SNR improvement achieved with SLSC beamforming resulted in greater SNR values even for dark skin colors, when compared with the conventional amplitude-based FFT PA imaging approach.

IV. Conclusion

This work is the first to demonstrate improvements in signal visibility achieved with SLSC beamforming applied to various skin tones. In particular, SNR decreased with epidermal melanin content and increased with optical wavelength for both conventional amplitude-based and SLSC PA images. In addition, clutter artifacts were identified as a critically responsible for the degraded quality of conventional amplitude-based PA images acquired with an optical wavelength of 750 nm, particularly for subjects with darker skin tones. However, SLSC beamforming successfully reduced the presence of incoherent acoustic clutter. Therefore, improved SNR was achieved with SLSC beamforming when compared to conventional amplitude-based PA imaging, resulting in better image quality and improved visualization of the radial artery. Moreover, the SLSC images of volunteers with the dark skin tone achieved comparable SNR to that obtained with a combination of light skin tone and conventional amplitude-based PA imaging.

References

[1] J. H. Uliana, D. R. T. Sampaio, G. S. P. Fernandes, M. S. Brassesco, M. H. Nogueira-Barbosa, A. A. O. Carneiro, and T. Z. Pavan, "Multi-angle long-axis lateral illumination photoacoustic imaging using linear array transducer," *Sensors*, vol. 20, p. 4052, 2020.

[2] Y. Wang, Y. Zhan, M. Tiao, and J. Xia, "Review of methods to improve the performance of linear array-based photoacoustic tomography," *Journal of Innovative Optical Health Sciences*, vol. 13, pp. 1–12, 2020.

[3] S. L. Jacques, "Optical properties of biological tissues: a review," *Physics in Medicine & Biology*, vol. 58, no. 11, p. R37, 2013.

[4] A. N. Bashkatov, E. A. Genina, and V. V. Tuchin, "Optical properties of skin, subcutaneous, and muscle tissues: A review," *Journal of Innovative Optical Health Sciences*, vol. 4, pp. 9–38, 2011.

[5] S. Preisser, G. Held, H. G. Akarçay, M. Jaeger, and M. Frenz, "Study of clutter origin in in-vivo epi-optoacoustic imaging of human forearms," *Journal of optics*, vol. 18, no. 9, p. 094003, 2016.

[6] Y. Mantri and J. V. Jokerst, "Impact of skin tone on photoacoustic oximetry and tools to minimize bias," *Biomedical Optics Express*, vol. 13, p. 875, 2 2022.

[7] X. Li, U. S. Dinish, J. Aguirre, R. Bi, K. Dev, A. B. E. Attia, S. Nitkunanantharajah, Q. H. Lim, M. Schwarz, Y. W. Yew, S. T. G. Thng, V. Ntziachristos, and M. Olivo, "Optoacoustic mesoscopy analysis and quantitative estimation of specific imaging metrics in fitzpatrick skin phototypes ii to v," *Journal of Biophotonics*, vol. 12, 9 2019.

[8] M. A. Lediju, M. J. Pihl, J. J. Dahl, and G. E. Trahey, "Quantitative assessment of the magnitude, impact and spatial extent of ultrasonic clutter," *Ultrasonic Imaging*, vol. 30, no. 3, pp. 151–168, 2008.

[9] S. Bjaerum, H. Torp, and K. Kristoffersen, "Clutter filter design for ultrasound color flow imaging," *IEEE transactions on ultrasonics, ferroelectrics, and frequency control*, vol. 49, pp. 204–216, 2002.

[10] G. Zwirn and S. Akselrod, "Stationary clutter rejection in echocardiography," *Ultrasound in medicine and biology*, vol. 32, pp. 43–52, 2006.

[11] S. Miyashita, "Efficacy of dynamic flow ultrasonography in fetal vascular imaging," *Med. Rev*, vol. 27, pp. 20–25, 2003.

[12] S. Huber, M. Wagner, M. Medl, and H. Czembirek, "Real-time spatial compound imaging in breast ultrasound," *Ultrasound in medicine and biology*, vol. 28, pp. 155–163, 2002.

[13] M. K. A. Singh and W. Steenbergen, "Photoacoustic-guided focused ultrasound (pafusion) for identifying reflection artifacts in photoacoustic imaging," *Photoacoustics*, vol. 3, pp. 123–131, 2015.

[14] H. C. Jo and D. Y. Kim, "Correlation between light absorbance and skin color using fabricated skin phantoms with different colors," *Lasers in Medical Science*, vol. 35, pp. 919–926, 6 2020.

[15] B. C. K. Ly, E. B. Dyer, J. L. Feig, A. L. Chien, and S. D. Bino, "Research techniques made simple: Cutaneous colorimetry: A reliable technique for objective skin color measurement," *Journal of Investigative Dermatology*, vol. 140, pp. 3–12.e1, 1 2020.

[16] M. T. Graham and M. A. L. Bell, "Photoacoustic spatial coherence theory and applications to coherence-based image contrast and resolution," *IEEE Transactions on Ultrasonics, Ferroelectrics, and Frequency Control*, vol. 67, pp. 2069–2084, 10 2020.

[17] M. A. Lediju, G. E. Trahey, B. C. Byram, and J. J. Dahl, "Short-lag spatial coherence of backscattered echoes: Imaging characteristics," *IEEE Transactions on Ultrasonics, Ferroelectrics, and Frequency Control*, vol. 58, pp. 1377–1388, 2011.

[18] M. A. L. Bell, N. Kuo, D. Y. Song, and E. M. Boctor, "Short-lag spatial coherence beamforming of photoacoustic images for enhanced visualization of prostate brachytherapy seeds," *Biomedical optics express*, vol. 4, no. 10, pp. 1964–1977, 2013.

[19] B. Pourebrahimi, S. Yoon, D. Dopsa, and M. C. Kolios, "Improving the quality of photoacoustic images using the short-lag spatial coherence imaging technique," in *Photons Plus Ultrasound: Imaging and Sensing 2013*, vol. 8581, pp. 680–685, SPIE, 2013.

[20] M. A. L. Bell, N. P. Kuo, D. Y. Song, J. U. Kang, and E. M. Boctor, "In vivo visualization of prostate brachytherapy seeds with photoacoustic imaging," *Journal of biomedical optics*, vol. 19, no. 12, p. 126011, 2014.

[21] M. A. L. Bell, X. Guo, H. J. Kang, and E. Boctor, "Improved contrast in laser-diode-based photoacoustic images with short-lag spatial coherence beamforming," in *2014 IEEE International Ultrasonics Symposium*, pp. 37–40, IEEE, 2014.

[22] E. A. Gonzalez and M. A. L. Bell, "GPU implementation of photoacoustic short-lag spatial coherence imaging for improved image-guided interventions," *Journal of Biomedical Optics*, vol. 25, no. 7, p. 077002, 2020.

[23] B. E. Treeby and B. T. Cox, "k-wave: Matlab toolbox for the simulation and reconstruction of photoacoustic wave fields," *Journal of Biomedical Optics*, vol. 15, p. 021314, 2010.